Fuel 404 (2026) 136286

Contents lists available at ScienceDirect

Fuel

journal homepage: www.elsevier.com/locate/fuel

Full Length Article

N-Octylaminopropan-2-ol surfactant for crude-oil asphaltene dispersion: Integrated experimental and modeling insights

Ulviyya J. Yolchuyeva [a,b,*], Vagif M. Abbasov [a], Orhan R. Abbasov [c], Yusif Abdullayev [a,d,f], Rena A. Jafarova [a], Ayaz M. Mammadov [a,e], Ravan A. Rahimov [d,a,b], Gunay A. Hajiyeva [a], Jochen Autschbach [g]

[a] Institute of Petrochemical Processes of Ministry of Science and Education Republic of Azerbaijan, Khojali ave. 30, Baku, Azerbaijan
[b] Department of Chemical Engineering, School of Engineering and Applied Science, Khazar University, 41 Mahsati Str., Baku, Azerbaijan
[c] Institute of Geology and Geophysics of the Ministry of Science and Education of the Republic of Azerbaijan, H. Javid ave. 119, Baku, Azerbaijan
[d] Department of Chemical Engineering, Baku Engineering University, Hasan Aliyev str. 120, Baku, Absheron AZ0101, Azerbaijan
[e] Sumgayit State University, Department of Chemistry, AZ 5008, 1Baku str., Sumgayit, Azerbaijan
[f] Division of Mathematics and Natural Sciences, Allen University, 1530 Harden St. Columbia, SC 29204, United States
[g] Department of Chemistry, University at Buffalo, State University of New York, Buffalo, NY 14260-3000, United States

ARTICLE INFO

Keywords:
Amino alcohol
Inhibition
Dispersion
Adsorption
NOSY NMR
DFT

ABSTRACT

This study provides the first-reported evidence that aliphatic structured surfactant, N-octylaminopropan-2-ol (OSI), is a novel and effective inhibitor of the aggregation of acidic, island-structured crude oil asphaltenes (A-ZO). The molecular mechanisms of OSI's effective dispersion were elucidated using a combination of advanced spectroscopic techniques and Density Functional Theory (DFT) calculations. Fourier Transform Infrared Spectroscopy (FT-IR) and Nuclear Magnetic Resonance (NMR) analyses revealed strong interactions between OSI and A-ZO, including hydrogen bonding and acid-base interactions, which prevent asphaltene precipitation in crude oil. Differential Thermal Analysis (DTA) confirmed the chemisorption of 12.5 % OSI onto A-ZO. Dynamic Light Scattering (DLS) measurements showed a significant reduction in the average nanosize of A-ZO in hexane, decreasing from 583 nm to 76 nm after treatment with OSI. Scanning Electron Microscopy (SEM) images of the A-ZO and OSI mixture revealed the filling of deep grooves and cracks on the rough surface of the asphaltene agglomerates, demonstrating the resin-like dispersion effect of OSI. DFT simulation reveals a binding energy of −28.2 kcal/mol for A-ZO and OSI complex formation. Noncovalent interaction (NCI) analysis shows that van der Waals interactions occur [$\mathrm{sign}(\lambda_2)\rho \approx -0.015$ to $+0.005$ au] in a large region between the OSI saturated tail and the A-ZO polycyclic aromatic fragment, which explains experimentally observed well-disperssed state of the hexane + A-ZO mixture after the addition a certain amount of OSI. The detailed, data-driven analysis offers unique molecular-level insights into asphaltene stabilization, presenting OSI as a significant alternative to traditional inhibitors for the oil industry.

1. Introduction

Asphaltenes deposition is one of the drawbacks that reduce oil field productivity [1,2] by clogging wells [3] and deteriorating reservoir rock properties [4,5]. It also leads to undesirable situations such as pipeline contamination [6,7] and increases the density and viscosity of hydrocarbons during oil transportation [8,9] and refining [10,11]. In this context, studying the aggregation process that leads to asphaltene deposition and its mitigation using effective inhibitors (dispersants) is of particular relevance for both Azerbaijani and global applications [12].

To address the above-mentioned oil production and transportation limitations, the asphaltene physical properties and structure have been extensively studied: asphaltene is insoluble in crude oil and low-molecular-weight alkanes (n-pentane, n-hexane, and n-hexane, etc.) [13,14], but soluble in light aromatic hydrocarbons (toluene, benzene, pyridine, etc.) [15,16]. Its molecular structure contains heavy metals (notably V + Ni: 0.0049–0.1795 %) and heteroatoms (N: 1–1.5 %, O: 7–14 %, S: 0.1–0.4 %) [17–19]. The asphaltene structure mainly consists

* Corresponding author at; Institute of Petrochemical Processes of Ministry of Science and Education Republic of Azerbaijan, Khojali ave. 30, Baku, Azerbaijan.
E-mail address: u.jeyhunzade@gmail.com (U.J. Yolchuyeva).

https://doi.org/10.1016/j.fuel.2025.136286
Received 29 April 2025; Received in revised form 4 June 2025; Accepted 15 July 2025
Available online 21 July 2025
0016-2361/

of condensed polyaromatic rings with alkyl chains and cycloparaffins [20,21]. The complex supramolecular asphaltene structure, known as the heaviest and most polar oil component, is described by two main models: the island model and the archipelago model [22]. In the island model, alkyl chains substitute around polycyclic aromatic core, while in the archipelago model, these cores are interconnected by alkyl chains [23–27]. The weak interactions between asphaltene molecules (e.g. van der Waals, hydrogen bonding, and π-π interactions) play a crucial role in the asphaltene precipitation/deposition [28–32].

Many approaches have been proposed to prevent asphaltene deposition [33,34], but only two methodologies have been widely utilized: mechanical and the chemical treatments. Applying mechanical methods is not feasible because of the high costs and the long time required for effectiveness. Chemical treatment relies on the use of inhibitors such as polymers, surfactants, ionic liquids, organic solvents, and nanoparticles [35,36]. The application of anionic and non-anionic surfactants as inhibitors leads to the formation of new steric interactions between the solvent and asphaltene aggregates [37,38]. In particular, the dissolution of the surfactant inhibitor in the solvent results in complex salt formation because of the acidic and basic nature of the components (asphaltene and surfactant) [39–46]. The effectiveness of anionic and non-anionic inhibitors depends on their polarity and molecular structure, but their ability to disperse asphaltenes can be reduced if amphiphilic molecules cluster together instead of interacting with asphaltene aggregates [47–49]. In certain cases, asphaltene clustering can hinder interactions with the dispersant and obstruct the steric protection provided by alkane chains.

Surfactants such as cetyltrimethylammonium bromide (CTAB), sodium dodecyl sulfate (SDS), Triton X-100, etc., prevent asphaltene aggregation by reducing intermolecular interactions. Cationic surfactants (e.g., CTAB) disrupt asphaltene molecules through electrostatic repulsion and bind to their acidic groups. Anionic surfactants (e.g., SDS) reduce asphaltene aggregation by creating hydrophilic interactions and imparting a negative charge on the surface of asphaltene particles. Nonionic surfactants (e.g.,Triton X-100) stabilize asphaltene particles in solution by forming a protective monolayer around them [50–58]. However, several factors can reduce the effectiveness of these surfactants, including their tendency to foam, interactions with other crude oil components (e.g., resins and salts), high asphaltene concentrations, and elevated thermobaric conditions [59–65]. These limitations can lead to various technological issues, such as corrosion and contamination of pipelines and equipment.

Benzoyl and salicylic acids, as inhibitors, exhibit aromatic solubility and facilitate π-π and acid-base interactions, which help to mitigate asphaltene aggregation and precipitation. However, their high toxicity, prolonged environmental stability (leading to corrosion), and tendency to form undesirable compounds with metal ions present significant limitations [66–68].

An analysis of previous studies [69–73] revealed that asphaltene inhibitors based on dodecylbenzene sulfonic acid (DBSA), ethoxylated nonylphenols, salicylic acid, and vegetable oils exhibited varying inhibition effects on the same oil sample. DBSA was found to be more effective in asphaltene structures containing basic functional groups. Depending on the properties of the asphaltene, the inhibitory effect of sulfonic acids can be positive or negative. The interaction between the high molecular weight asphaltenes and the inhibitor, through hydrogen bonding or acid-base complex formation, reduces the probability of asphaltene aggregation [62,74]. However, the precise nature and primary role of these interactions in asphaltene inhibition remain subjects of scientific debate. For instance, Subramanian et al. suggested that acid-base interactions play a secondary role, with the key mechanism, possibly involving hydrogen bonding or van der Waals forces, still needing precise identification [75]. Conversely, other studies, such as Zhang et al. indicate that acid-base reactions are indeed the most effective stabilizing mechanism, complemented by π-π interactions and hydrogen bonding [76]. This perspective is further supported by Kashefi et al. who reported that acid-containing inhibitors are particularly effective against basic asphaltene aggregation, achieving notable average particle size reductions: octyl phenol (55 %), synthesized deep eutectic solvent (41 %), lauric acid (24 %), and dodecyl amine (18 %) [77]. The higher inhibitory activity of nonylphenol compared to phenol is attributed to the influence of its long peripheral alkane chain, which enhances the polarity of the phenol OH functional group [78–80]. Some inhibitors (e.g. resins, maltenes, etc.) do not demonstrate the same dispersing properties as phenol and ethoxylated alcohols at low doses (ppm) [81–83].

Crude oil resins are considered naturally available inhibitors that prevent asphaltene clustering by providing stability to polar molecules in a non-polar environment. A reduction in resin content has been found to promote asphaltene aggregation and flocculation. Aliphatic solvents cause resin desorption, further enhancing aggregation and flocculation. To limit asphaltene deposition, dispersants were typically selected based on the resin properties. Their effectiveness depends on their interaction with polar groups of the asphaltene molecules and their adsorption onto the surface of asphaltene aggregate [84–92].

DLS and DFT studies are pivotal for understanding asphaltene aggregation and inhibitor mechanisms [93–99]. For instance, studies on carbon nanoparticles used to counter asphaltene aggregation in unstable crude oils revealed that the average nanosize of asphaltene aggregates adsorbed onto carbon nanoparticles reduced from 1730 nm to 255 nm, and in addition to strong hydrogen bonding and π–π interactions can form between carbon nanoparticles and asphaltene molecules [100]. Kumar et al. investigated asphaltene aggregation in thymol-based deep eutectic solvents using DFT and found that thymol-diphenyl ether exhibited a higher solubility for asphaltenes [101]. Chávez-Miyauchi et al. showed that N-aryl amino-alcohols, particularly boronic acid derivatives with Lewis acid characteristics, have been shown to inhibit asphaltene aggregation by forming stable tetrameric complexes. DFT calculations and experimental studies identified that longer alkyl chains enhance dispersion and inhibition efficiency [102].

Findings from the published literature indicated that several factors-including molecular structure, polarity, solvent solubility, adsorption, dosage, hydrogen bonding, and acid-base interactions-influence the efficacy of the listed inhibitors. In this study, we evaluate the performance of the proposed basic surfactant, N-octylaminopropan-2-ol (OSI), against island-structured acidic asphaltene molecules extracted from crude oil, considering the key properties previously tested. Our research provides comprehensive insights into the molecular behavior of this new, effective inhibitor. The proposed surfactant effectively inhibits asphaltene aggregation and deposition in crude oil and represents a simply synthesizable alternative to existing inhibitors in the oil industry.

2. Materials and methods

All chemicals used in this study were of analytical grade: n-hexane (≥99 %, Cat. No. 296090) and toluene (≥99.5 %, Cat. No. 244511) from Sigma-Aldrich; octylamine (98 %, Cat. No. 00625) and propylene oxide (≥99 %, Cat. No. 04010) for OSI synthesis from Sigma-Aldrich; and deuterated chloroform ($CDCl_3$, Cat. No. 151823) for NMR from Merck.

The intermolecular interactions between A-ZO and OSI were studied using FT-IR spectroscopy (BRUKER) in the spectral range of 400–4000 cm^{-1} with a resolution of 2 cm^{-1}, using a zinc selenide crystal at room temperature.

The possible interactions in A-ZO + OSI complex were tracked using ^1H and NOESY NMR spectra in a BRUKER-Fourier spectrometer (300 MHz) at room temperature. Tetramethylsilane was used as an internal standard, and deuterated chloroform was applied as a solvent.

OSI adsorption on the A-ZO surface were determined using a thermogravimetric analyzer (TG/DTG mode) of the NETZSCH STA449F3 Jupiter system in a temperature-programmed dynamic mode, at the temperature range of 23–1000 °C with a temperature rise rate of 10 K/min, and in an inert environment. The flow rate of the inert gas (N_2) was

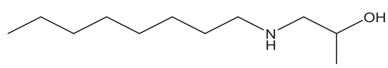

N-Octylaminopropan-2-olsurfactant inhibitor (OSI)

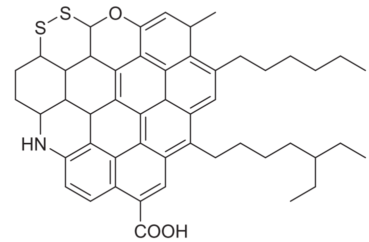

Asphaltene from Zaghli field oil (A-ZO)

Fig. 1. Molecular structures of OSI and A-ZO.

20 ml/min, and the sample amount was ~ 10 mg. Prior to TG-DTG measurements, vacuum pumping was employed in the sample chamber to remove residual oxidative gases.

The change in asphaltene particle size in the A-ZO + OSI mixture was studied using HORIBA LB 550 DLS. Measurements were performed before and after the addition of OSI to the A-ZO-hexane and −toluene solutions/mixtures at 298 K, using a laser diode light source with a wavelength of 650 nm and a power of 5 mW. The measurement range is between 1 nm–6 μm.

For the morphological characterization of the A-ZO, A-ZO and OSI mixture, a Hitachi S-3400 N SEM with an OXFORD Instruments atomic analyzer was used. The measurements were performed at an accelerating voltage of 1–2 kV, a working distance of 6–7 mm and a magnification range of 50-500x. A secondary electron detector and high vacuum mode were used for the measurements.

All measurements were repeated in triplicate, with mean values reported to ensure data reproducibility and reliability.

The asphaltene (A-ZO) used in the experiments was extracted from the oil of the Zaghli field in East Azerbaijan, following the ASTM D6560-12 standard [103]. The (A-ZO) structure was fully elucidated and reported in our previous work [104]. The structure of A-ZO and synthesized N-Octylaminopropan-2-ol inhibitor (OSI) is shown in Fig. 1.

It has been determined that the A-ZO cluster is a heterostructured (S-S, C-S, and N–H bonds) molecule containing polycyclic aromatic components, alkyl, cycloalkyl fragments, and a COOH group. According to its structural model, this asphaltene is classified as an "island" type, with approximately 50 % aromatic hydrocarbons in its composition [104].

The OSI is a yellowish, transparent, viscous liquid, synthesized based on the reaction of octylamine and propylene oxide (1:1). The synthesized product (OSI) is soluble in water, ethanol, acetone, hexane, kerosene, CCl_4, and isopropanol. The OSI amine value was calculated as 289.2 mg KOH/g [105].

The A-ZO to OSI ratio in the conducted experiments was adjusted to 1:0.1, respectively. 5 % solutions of A-ZO were prepared using two solvents: toluene and hexane. In a hexane solution, A-ZO precipitates immediately, whereas in toluene, precipitation occurs after 90 min. The incorporation of 5000 ppm of OSI into the A-ZO solutions resulted in a stable suspension in hexane. However, no precipitation was observed in the toluene solvent during a 10-hour monitoring period.

The Gaussian 16 program [106] was utilized for the optimization of surfactant, asphaltene and surfactant and asphaltene complex structures. For the optimizations, Kohn-Sham DFT with the B3LYP functional [107] and D3BJ dispersion corrections [108] was used. The 6-311G(d,p) basis set was employed for all atoms. Solvent effects were considered via

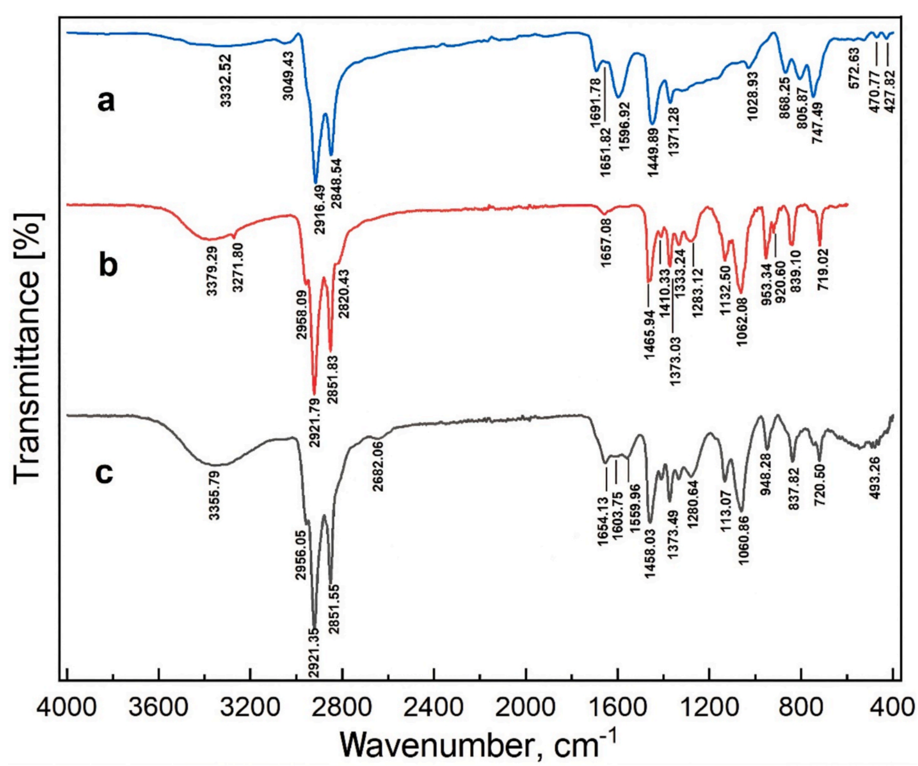

Fig. 2. FITR spectra of A-ZO (a), OSI (b), and their mixture (c).

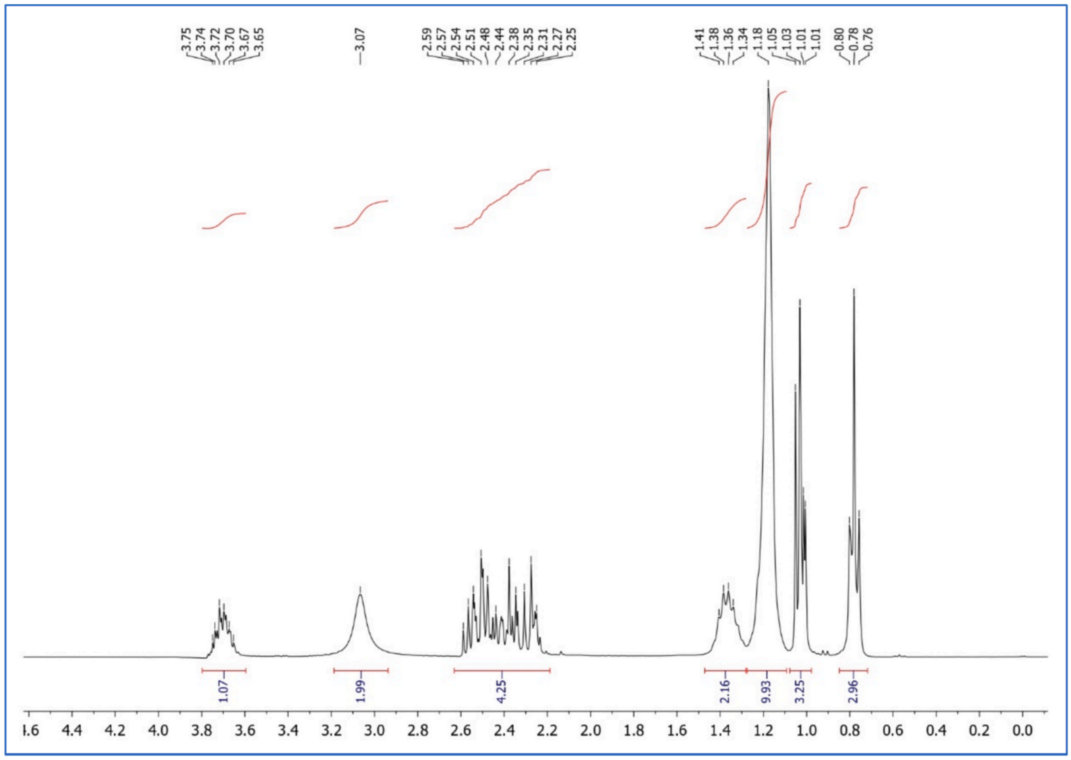

a)

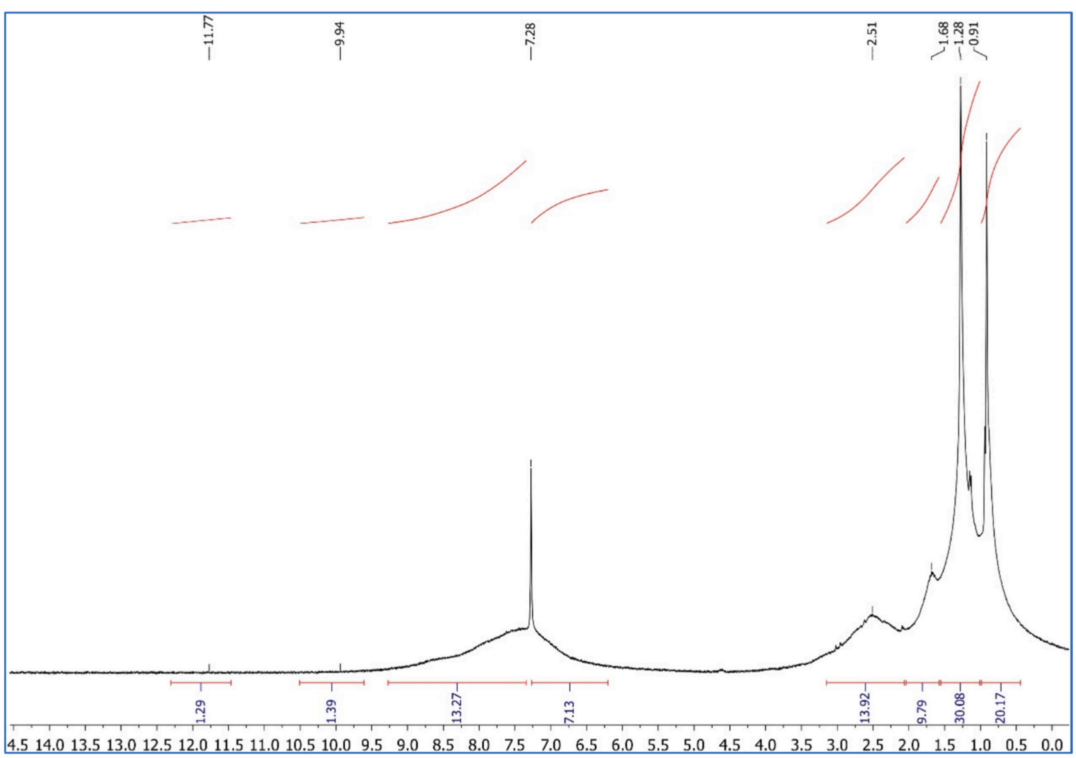

b)

Fig. 3. ^{1}H NMR (a, b, c) and NOESY NMR (d) spectra of OSI (a), A-ZO (b), and their mixture (c, d).

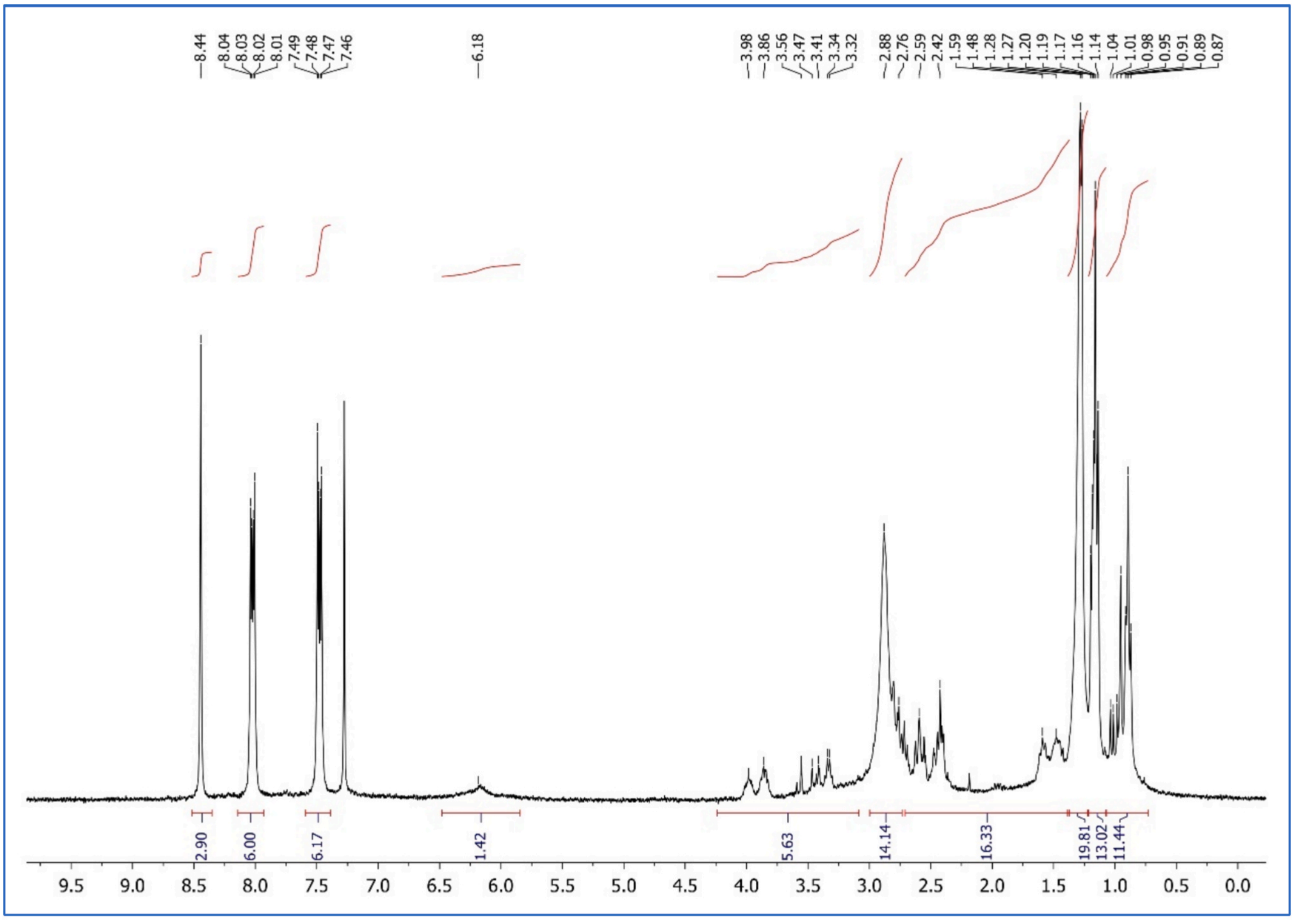

c)

Fig. 3. (*continued*).

a self-consistent reaction field and default polarizable continuum model with the dielectric constant for n-hexane (ε = 1.8819). Gibbs energies were calculated at 298.15 K to reflect the experimental room temperature conditions. Optimized geometries (in XYZ format, See SI, Table S1, S2) of A-ZO are provided in the electronic supporting information (ESI). The A-ZO + OSI complex binding energy (E_b) was calculated according to the equation: $E_b = E_{OSI+A-ZO} - (E_{OSI} + E_{A-ZO})$ where $E_{OSI+A-ZO}$ stands for the total energy of the complex, while E_{OSI} and E_{A-ZO} are individual total energies of OSI and A-ZO, respectively. Binding energy of the A-ZO + OSI was corrected using basis set superposition error (BSSE) according to the counterpoise method [109]. The formchk file of the optimized A-ZO + OSI was utilized as input in Multiwfn 3.8 [110] to generate NCI analysis based on the reduced density gradient (RDG) and sign(λ_2)ρ. The data were then visualized with Gnuplot 6.0 program package [111] to design a 2D plot (RDG vs. sign(λ_2)ρ). VMD 4 [112] was used to construct the 3D isosurface colored according to sign (λ_2)ρ. This integrated computational and visualization approach enabled a comprehensive assessment of the NCI interactions in the system.

3. Results and discussions

The FT-IR spectra of OSI, A-ZO and A-ZO + OSI mixturewere shown in Fig. 2.

The C–H absorption bands for bending and stretching vibrations in the –CH_3 and –CH_2 groups were observed at 1371, 1373, 1410, 1449, 1465, and 2820, 2848, 2851, 2916, 2921, and 2958 cm^{-1}, respectively for the A-ZO and OSI structures (Fig. 2a and 2b). The bending vibrations of the C–H bond in aromatic hydrocarbons appear at 747, 805, and 868 cm^{-1}, the stretching vibration of the =C–H bond at 3049 cm^{-1}, and the C=C bond stretching vibration at 1596 cm^{-1}. The C–O and C=O bonds stretching vibrations for the related acid functionality in A-ZO were observed at 1028 and 1691 cm^{-1}, respectively [113]. The absorption bands observed at 427, 470, 526 and 572 cm^{-1} are related to S–S and C–S bonds. The absorption maximum at 1651 cm^{-1} corresponds to the bending vibration of the N–H bond, while the 3332 cm^{-1} absorption band shows overlapping stretching vibrations of the N–H and O–H bonds of the acid (Fig. 2a) [114]. The absorption maxima at 1062, 1132 and 3379 cm^{-1} correspond to the stretching vibrations of the C–O and H–O bonds of the alcohol, respectively. The bending and stretching vibrations of the N–H bonds are observed at 1675 and 3271 cm^{-1}(Fig. 2b). The disappearance of the C=O band (1691 cm^{-1}) in the A-ZO + OSI spectrum (Fig. 2c) indicates interaction between the OSI amine functionality and the A-ZO carboxyl group. Two absorption maxima at 1559 and 2682 cm^{-1} are characteristic of the COO^- and $N\text{-}H^+$ groups [115,116]. The absorption maxima associated with N–H and O–H bonds in the spectral range of 3100–3700 cm^{-1} appear to overlap at 3355 cm^{-1} (Fig. 2c). The nature of the contour of this absorption band indicates its acidic character [117].

FT-IR results show that OSI has polar (NH and OH) and non-polar sides. The polar side binds to asphaltene molecules, while the non-polar aliphatic crown prevents aggregation through steric repulsion, keeping asphaltenes suspended [118]. The acid group in A-ZO enhances the effectiveness of OSI, stabilizing asphaltenes in crude oil.

In the ^{1}H NMR (δ, ppm) spectrum of OSI shown in Fig. 3a, the signals of hydrogen atoms are recorded at 0.78 ppm for the CH_2-$\underline{CH_3}$ (3H) group, and at 1.03 ppm for the CH-$\underline{CH_3}$ (3H) group, 1.09–1.29 ppm

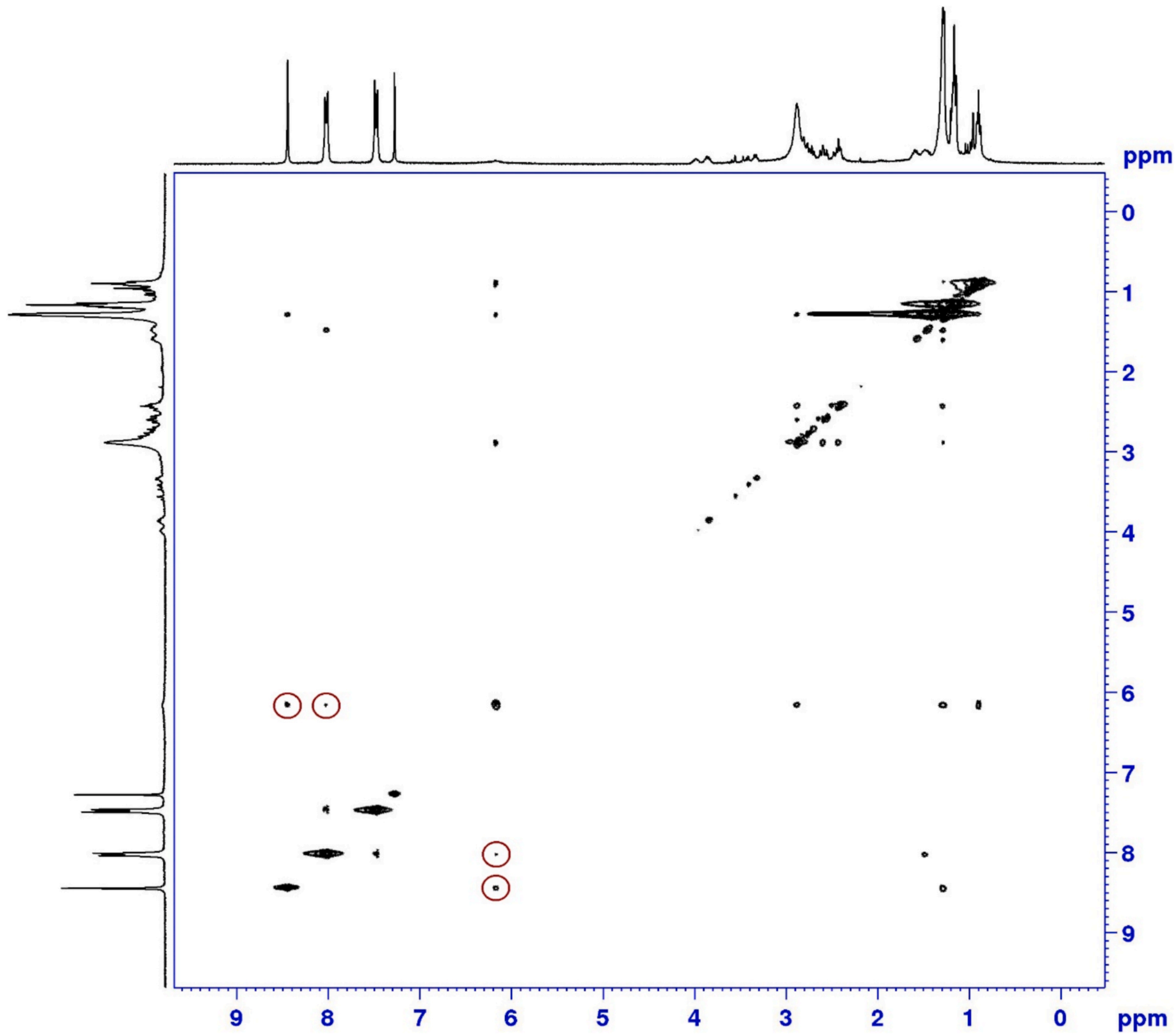

Fig. 3. (*continued*).

corresponds to the CH_2 (10*H*) group in the saturated hydrocarbon tail. 1.36 ppm for the <u>CH_2</u>-CH_2-NH (2H) group, 2.32–2.60 ppm for the <u>CH_2</u>-NH (4H) group, and 3.69 ppm for the <u>CH</u>-OH (1H) group. In that spectrum, an overlap of OH and NH signals is observed at 3.06 ppm (2H) [94].

As shown in Fig. 3c, some signals in the ^{1}H NMR spectrum overlap because the A-ZO + OSI sample contains similar fragments (–CH_2– and –CH_3). The CH_3 group is observed at 0.75–1.09 ppm, and the CH_2 group at 1.09–1.41 ppm. The β-CH– and –CH_2 groups, associated with naphthenic hydrocarbons and some hydroaromatic fragments of A-ZO, appear between 1.41–1.90 ppm (Fig. 3b). The <u>CH_2</u>-CH_2-NH group from OSI is seen at 1.30–1.46 ppm, but its signal is not clearly distinguishable (Fig. 3c). The 2.30–2.70 ppm range corresponds to –CH_3 groups bonded to the aromatic ring in A-ZO and the <u>CH_2</u>-NH groups of OSI. Hydrogen atoms from > CH– and –CH_2 groups attached to the aromatic nucleus are detected between 2.70–3.42 ppm, linked to A-ZO. The OSI OH group shows a resonance at 2.88 ppm, while the CH-OH group appears between 3.75–4.11 ppm. The proton signals in polyaromatic ring are observed at 7.47, 8.01, and 8.44 ppm. The most notable feature in Fig. 3c is the shift of the NH group signal to 6.16 ppm, caused by hydrogen bonding between the NH group of OSI and the A-ZO molecule [104,119–126].

The NOSY spectrum of the A-ZO + OSI sample (Fig. 3d) shows that the OH group signal correlates with the NH group signal (2.88–6.16 ppm). The signals observed in the 2.30–2.70 ppm range (CH_2-NH) correspond to OSI. The hydrogen atoms of the polyaromatic nuclei exhibit correlations both with each other (7.47–8.01 ppm) and with the alkyl groups (8.01–1.48 ppm and 8.44–1.27 ppm). Additional correlations are observed in the CH_2 signal recorded at 1.27 ppm. This signal correlates with both the alkyl fragments (1.48 and 1.59 ppm) and the OH and NH groups, indicating interactions within the OSI and A-ZO complex. Since both A-ZO and OSI molecules contain a saturated chain (CH_2), these signals cannot be clearly separated. In the NOESY spectrum, the correlation between the NH signal (6.16 ppm) and aromatic hydrogens (8.44 ppm, strong; 8.01 ppm, weak) is noteworthy. These correlations (6.16–8.44 ppm and 6.16–8.01 ppm) suggest the formation of hydrogen bonds between the A-ZO and OSI molecules [127,128]. The TG and DTG curves (Fig. 4a) revealed that the A-ZO molecule is thermostable up to 406 °C. The three-stage pyrolysis process, occurring between 406–818 °C, ends with the formation of 12.58 % coke. Endothermic peaks are associated with degradation reactions, while exothermic peaks correspond to internal oxidation or condensation.

Analysis of the TGA curve in Fig. 4b showed that the mass loss of OSI starts at approximately 207 °C and continues until 309 °C. This

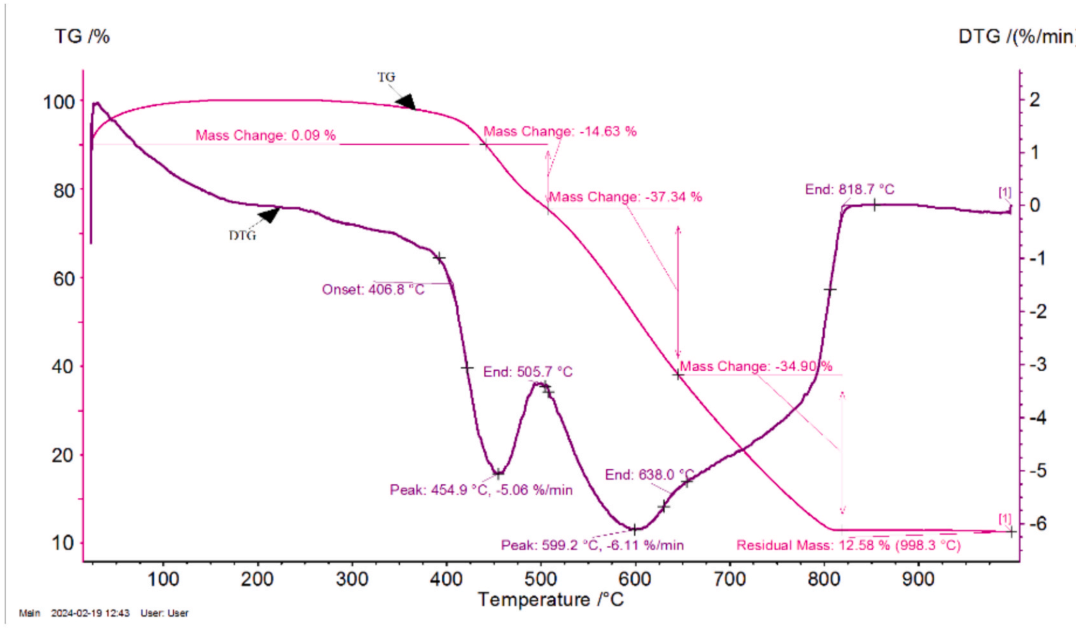

a)

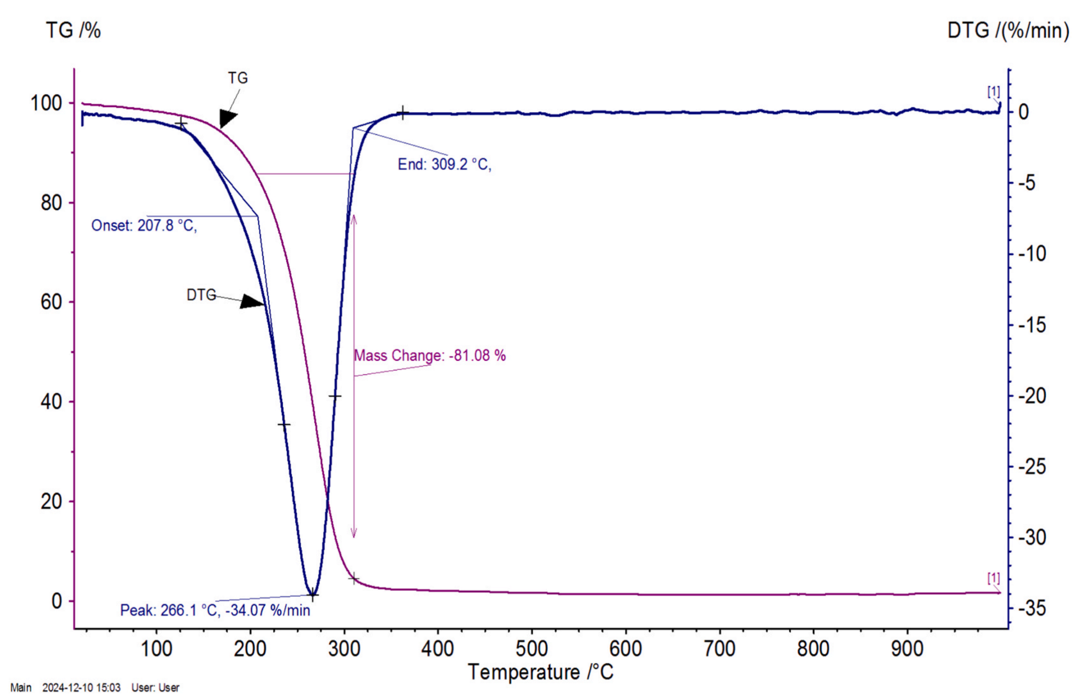

b)

Fig. 4. TGA and DTG mass loss curves of: A-ZO (a), OSI (b), and their mixture (c).

endothermic process ends with the formation of 0.01 % coke, indicating the thermostability of OSI up to 207 °C [129].

In Fig. 4c, the endothermic peak (297 °C) recorded in the temperature range 240–400 °C for the mixture of A-ZO and OSI was associated with the decomposition reaction of OSI, resulting in a mass loss of 12.5 %. This mass loss corresponds to OSI being chemisorbed by A-ZO. On the other hand, the thermal process occurring in the temperature range of 400–998 °C ends with the coking of A-ZO (16.77 %). The difference in the decomposition temperature of the mixture of A-ZO and OSI from the initial components may be due to their chemisorption. The formation of a new bond during the adsorption of OSI on A-ZO leads to an increase in its decomposition temperature [100,130,131].

DLS was used to study the effect of OSI on the change in aggregate sizes in A-ZO solutions in hexane and toluene. Figs. 5a and 5b show the changes in the distribution of A-ZO particles in solvents before and after the addition of OSI [104,132,133].

The 583 nm peak observed in Fig. 5a (1) corresponds to large clustered aggregates of A-ZO in hexane. Such aggregates precipitate rapidly in that solvent. However, when OSI is added to the hexane solution, the diameter of the aggregates decreases to 76 nm, and the degree of

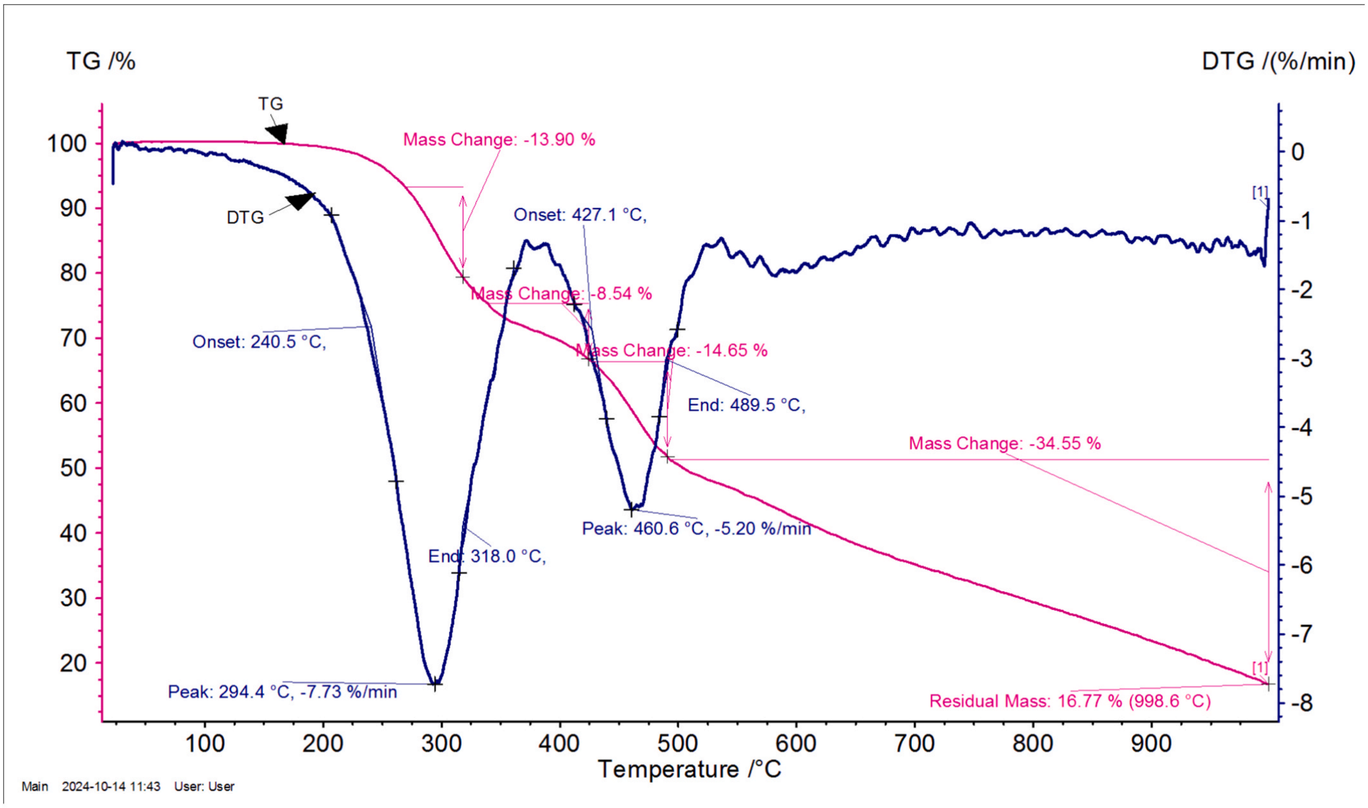

c)

Fig. 4. (*continued*).

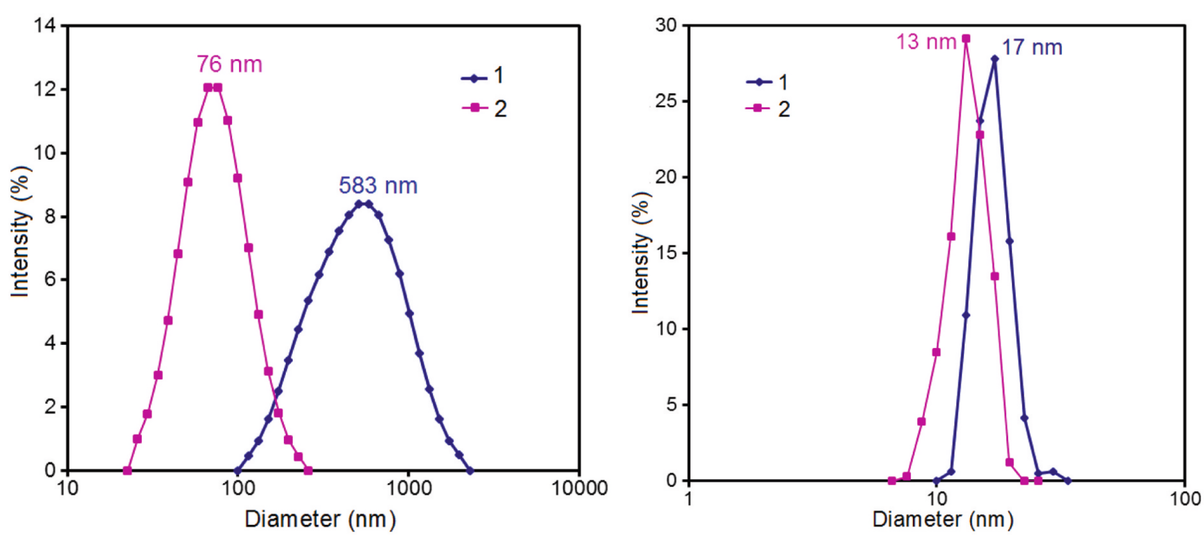

a) *b)*

Fig. 5. DLS curves of A-ZO (1) and A-ZO + OSI mixture (2) in hexane (a) and toluene (b) solvents.

dispersion increases approximately 7 times (Fig. 5a (2)).

The diameter of A-ZO (Fig. 5b (1)) particles dissolved in toluene is 17 nm (Fig. 5b). This solution has a high monodispersity. When OSI is added to it, the monodispersity is almost unchanged, and the particle size decreases to 13 nm.

Our identification reveals that the increase in the size of aggregates in a hexane solution is due to the intermolecular interaction of aromatic nuclei in A-ZO. In this solution, the interaction of A-ZO molecules with OSI increases the polarity of the medium and causes suspension. A π-π interaction occurs between the aromatic rings of A-ZO and the aromatic nucleus of toluene solvent in the solution, which results in monodispersity. When OSI is added to the solution, A-ZO molecules are disaggregated and do not settle for a long time (approximately 10 h).

Fig. 6 depicts the suspension process that occurs after the addition of OSI to A-ZO solution, along with the precipitation of A-ZO in hexane.

In our experiments, the approximately 90 % decrease in the average

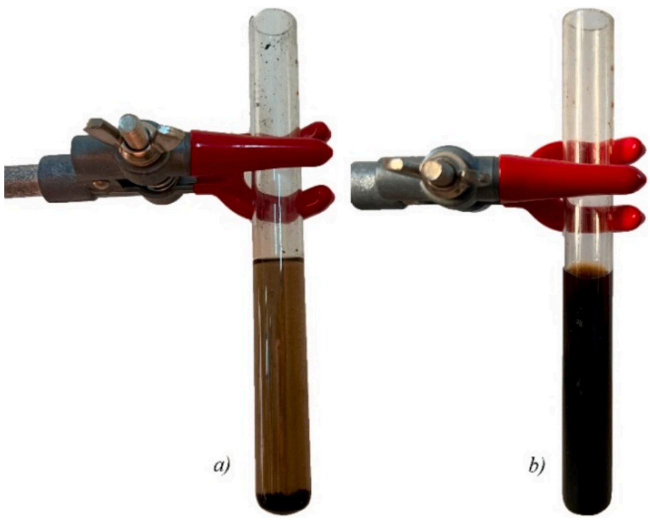

Fig. 6. Visual demonstration of A-ZO deposition in hexane solution (a) and its stabilization after OSI addition (b).

size of aggregates with the addition of OSI is explained by the increase in acid-base, electrostatic, polar, and van der Waals interactions between OSI and A-ZO molecules.

In the micrograph shown in Fig. 7a, A-ZO consists of agglomerates of various shapes and sizes (averaging 247 and 124 μm) with a flaky, brittle surface. Cracks are observed on the surface of A-ZO aggregates, resulting from the separation of the resin fraction. Fig. 7b demonstrates significant agglomerate shrinkage (to ~ 2.68 μm) in the A-ZO/OSI complex, along with smoothing of cracks and filling of voids, consistent with DLS-reported size reduction. These morphological changes confirm OSI's resin-like role in stabilizing and dispersing aggregated asphaltenes in crude oil [101,132,134,135].

The solvent phase BSSE corrected negative binding energy ($E_b = -28.2 kcal/mol$) indicates that the OSI molecules can be effective to suppress asphaltene aggregation, which is experimentally evident. The interaction between A-ZO and OSI was investigated in solvent phase to simulate experimental condition better. The optimizations were started with basic (the A-ZO carboxyl group) and acidic (the OSI carboxyl group) functionalities in spatial proximity to ensure their interactions in the resulting structure. The availability of carboxyl group in A-ZO and amine group in the OSI structures may result in electrostatic interaction between two components because of possible proton transfer from the

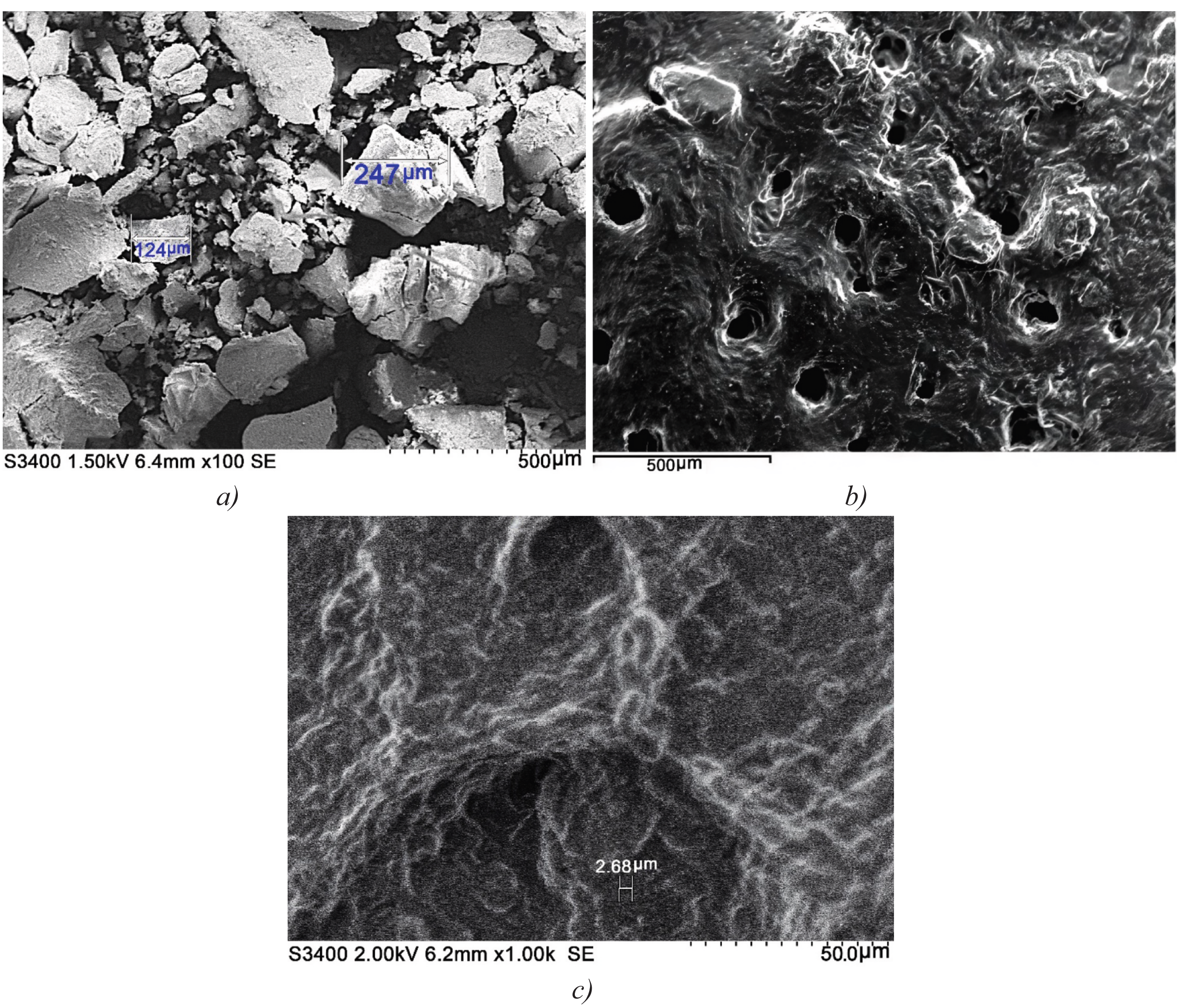

Fig. 7. SEM micrographs of A-ZO (a), and A-ZO + OSI mixture (b, c).

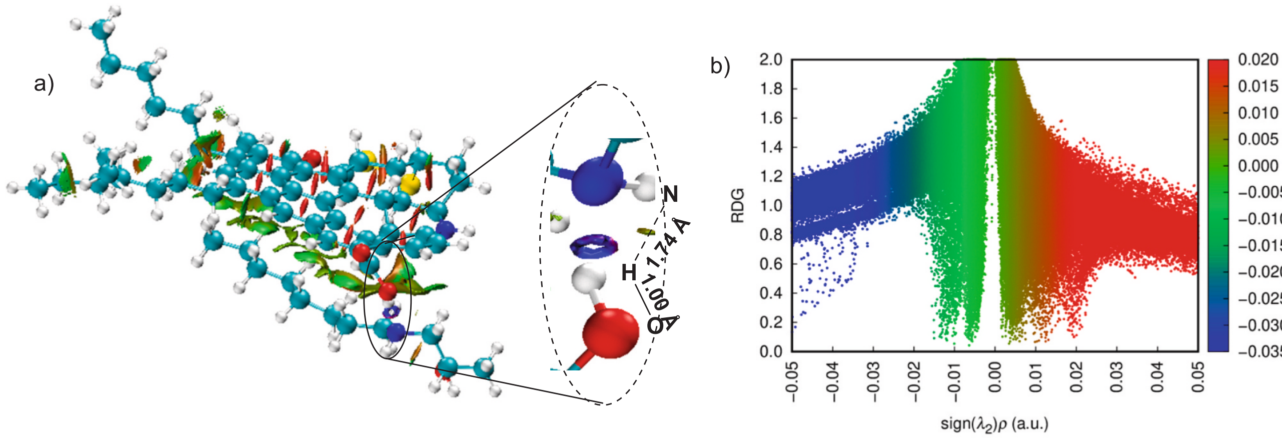

Fig. 8. A) Three-dimensional NCI isosurfaces of the a-zo + OSI complex, showing a small blue torus (magnified) that indicates hydrogen-bonding interaction. Green regions represent more dispersive attractive interactions. b) RDG and sign(λ_2)ρ plots for the studied system. The RDG isosurfaces were generated using a cutoff value of RDG = 2.0, with color coding based on sign(λ_2)ρ in the range −0.05 to + 0.05 au. Blue represents strong bonding interactions, green indicates dispersive attractive (vdW) interactions, and red corresponds to repulsive interactions (See SI, Fig. S1 for the visualized A-ZO and OSI stuructures from different prospective).

carboxylic part to the amine functionality. Analysis of optimized A-ZO + OSI complex showed that the interaction in nonpolar solvent (hexane) is not electrostatic, rather the O–H; 1.00 Å and H-N; 1.74 Å bond distances revealed that the interactions have hydrogen-bonding nature. In a primary acid-base interaction (primary amins, e.g., methylamine and ethylamine and acetic acid combinations), the N-H distance was calculated to be shorter (1.54–1.61 Å) [136]. In the A-ZO + OSI system, because of large A-ZO and OSI surfaces, non-covalent interactions (NCIs) place the molecules in a relative position that prevents proper hydrogen transfer and electrostatic interaction between amine and carboxylic functional groups in the A-ZO + OSI complex. The hydrogen-bonding character was further explored by NCI analysis. As seen in Fig. 8, there is a small blue torus-shaped isosurface located between H—N, which is an indication of hydrogen bonding. The corresponding hydrogen-bonding region in the two-dimensional NCI plot can be seen as blue dots in the region with sign(λ_2)ρ values in the range of −0.03 to −0.05 au (Fig. 8). van der Waals interactions [indicated by sign(λ_2)ρ ≈ −0.015 to + 0.005 au] occur between the OSI saturated tail and the A-ZO polycyclic aromatic regions where the electron density is very low (green isosurfaces, Fig. 8), and the RDG is high. Larger negative region (−0.05 au to −0.02) represents attractive ineractions.

4. Conclusion

The aggregation process of acidic A-ZO with island structure from crude oil was investigated using an integrative approach of FTIR, NMR, DTA, DLS, SEM and DFT methods to study the inhibitory effect of a newly synthesized surfactant, OSI. It was found that 12.5 % of OSI undergoes chemisorption on A-ZO, which is accompanied by a decrease in the average size of asphaltene aggregates by about 7 times. The polar and nonpolar parts of the OSI molecule interact with the asphaltene molecule, significantly slowing down the aggregation process and promoting the formation of a stable suspension due to steric repulsion. The presence of a carboxyl group in the A-ZO structure enhances the efficiency of the basic inhibitor. Formation of strong intermolecular interactions between the functional groups of the inhibitor and the active sites of asphaltene, including acid-base (COO^- and NH^+), hydrogen (bond energy of 28.2 kcal/mol) and van der Waals forces, is the main driving force that prevents aggregation and promotes asphaltene stabilization. Micrographs of the A-ZO and OSI complex demonstrate smoothing of the porous and flaky brittle surface of asphaltene agglomerates of various shapes and sizes, confirming strong interactions between them. This interaction elucidates OSI's resin-like functionality as a dispersing and stabilizing agent for aggregated asphaltenes in crude oil, demonstrating its capacity to prevent asphaltene deposition while presenting viable applications as a novel, high-performance industrial inhibitor.

CRediT authorship contribution statement

U.J.Yolchuyeva: Methodology, Investigation, Formal analysis, Writing – original draft, Resources, Project administration. **V.M. Abbasov:** Supervision, Funding acquisition. **O.R.Abbasov:** Writing – review& editing, Data curation. **Y.Abdullayev:** Writing – review& editing, Software. **R.A.Jafarova:** Supervision. **A.M.Mammadov:** Formal analysis, Data curation. **R.A.Rahimov:** Writing – review & editing, Data curation. **G.A.Hajiyeva:** Validation, **J Autschbach**: Writing – review & editing, Software.

Declaration of competing interest

The authors declare that they have no known competing financial interests or personal relationships that could have appeared to influence the work reported in this paper.

Acknowledgments

J.A. thanks The National Science Foundation, grant CHE-2503332 and its predecessor CHE-2152633, for support. All authors thank the Center for Computational Research (CCR, http://hdl.handle.net/10477/79221), University at Buffalo for providing computational resources. The authors express their deep gratitude to Nushaba Aliyeva, Head of the Laboratory for the Study of Catalysis Problems by Spectroscopic Methods, Institute of Petrochemical Processes of the Ministry of Science and Education of Azerbaijan, for her assistance in conducting DLS and DTA analyses.

Appendix A. Supplementary data

Supplementary data to this article can be found online at https://doi.org/10.1016/j.fuel.2025.136286.

Data availability

The authors are unable or have chosen not to specify which data has been used.

References

[1] Gharbi K, Benyounes K, Khodja M. Removal and prevention of asphaltene deposition during oil production: a literature review. J Pet Sci Eng 2017;158: 351–60. https://doi.org/10.1016/j.petrol.2017.08.062.

[2] Yang Z, Wu X, Guo J, Zhang J, Xiong R, Liu L, et al. Characterization of asphaltene deposition behavior in diluted heavy oil under high-pressure conditions. Energies 2023;16:6780. https://doi.org/10.3390/en16196780.

[3] Rastgoo A, Kharrat R. Investigation of asphaltene deposition and precipitation in production tubing. Int J Clean Coal Energy 2017;6:14–29. https://doi.org/10.4236/ijcce.2017.61002.

[4] Li L, Wang M, Su Y, Gao X, Wang W, Tu J, et al. Investigation of asphaltene precipitation and reservoir damage during CO_2 flooding in high-pressure, high-temperature sandstone oil reservoirs. SPE J 2024;29:4179–93. https://doi.org/10.2118/214805-PA.

[5] Farajollahi S, Bazvand M, Tahernejad E. Asphaltene deposition effects on reservoir rock wettability and modification strategies. Heliyon 2024;10:e38436. https://doi.org/10.1016/j.heliyon.2024.e38436.

[6] Adebiyi FM. An insight into asphaltene precipitation, deposition and management stratagems in petroleum industry. J Pipeline Sci Eng 2021;1: 419–27. https://doi.org/10.1016/j.jpse.2021.08.006.

[7] El Ghazouani J, Saidoun M, Tort F, Daridon JL. Experimental evaluation method of asphaltene deposition inhibitor's efficacity at atmospheric pressure using a fully immersed quartz crystal resonator, centrifugation, and optical microscopy techniques. Energy Fuels 2023;37:5895–904. https://doi.org/10.1021/acs.energyfuels.3c00305.

[8] Ghanema AA, Al-Sabagh AM, El-Kady MY, Desouky SEM, Betiha MA. Solutions of asphaltene deposition problems and their impacts on petroleum production. Int J Curr Res Chem Pharm Sci 2018;5:4–15. https://doi.org/10.22192/ijcrcps.

[9] Fakher S, Ahdaya M, Elturki M, et al. Critical review of asphaltene properties and factors impacting its stability in crude oil. J Petrol Explor Prod Technol 2020;10: 1183–200. https://doi.org/10.1007/s13202-019-00811-5.

[10] Alimohammadi S, Zendehboudi S, James L. A comprehensive review of asphaltene deposition in petroleum reservoirs: theory, challenges, and tips. Fuel 2019;252:753–91. https://doi.org/10.1016/j.fuel.2019.03.016.

[11] Guerrero-Martin CA, Montes-Pinzon D, Motta da Silva MM, Montes-Paez E, Guerrero-Martin LE, Salinas-Silva R, et al. Asphaltene precipitation/deposition estimation and inhibition through nanotechnology: a comprehensive review. Energies 2023;16:4859. https://doi.org/10.3390/en16134859.

[12] Nassar NN, Hassan A, Vitale G. Comparing kinetics and mechanism of adsorption and thermo-oxidative decomposition of Athabasca asphaltenes onto TiO_2, ZrO_2, and CeO_2 nanoparticles. Appl Catal A 2014;484:161–71. https://doi.org/10.1016/j.apcata.2014.07.017.

[13] Qu S, Shen W. Asphaltenes: Separations, structural analysis and applications. J Energy Chem 2019;34:186–207. https://doi.org/10.1016/j.jechem.2018.10.004.

[14] Nikookar M, Omidkhah MR, Pazuki GR, Mohammadi AH. An insight into molecular weight distributions of asphaltene and asphalt using gel permeation chromatography. J Mol Liq 2022;362:119736. https://doi.org/10.1016/j.molliq.2022.119736.

[15] Zendehboudi S, Shafiei A, Bahadori A, James LA, Elkamel A, Lohi A. Asphaltene precipitation and deposition in oil reservoirs – Technical aspects, experimental and hybrid neural network predictive tools. Chem Eng Res Des 2014;92:857–75. https://doi.org/10.1016/j.cherd.2013.08.001.

[16] Khalaf MH, Mansoori GA. A new insight into asphaltenes aggregation onset at molecular level in crude oil (an MD simulation study). J Petrol Sci Eng 2018;162: 244–50. https://doi.org/10.1016/j.petrol.2017.12.045.

[17] Yakubov MR, Milordov DV, Yakubova SG, et al. Concentrations of vanadium and nickel and their ratio in heavy oil asphaltenes. Pet Chem 2016;56:16–20. https://doi.org/10.1134/S0965544116010072.

[18] Poveda-Jaramillo JC, Molina-Velasco DR, Bohorques-Toledo NA, Torres MH, Ariza-León E. Chemical characterization of the asphaltenes from Colombian Colorado light crude oil. CT&F - Cienc Tecnol Futuro 2016;6(3):105–22.

[19] Leyva C, Ancheyta J, Berrueco C, Millán M. Chemical characterization of asphaltenes from various crude oils. Fuel Process Technol 2013;106:734–8. https://doi.org/10.1016/j.fuproc.2012.10.009.

[20] Vale MGR, Silva MM, Damin ICF, Sanches Filho PJ, Welz B. Determination of volatile and non-volatile nickel and vanadium compounds in crude oil using electrothermal atomic absorption spectrometry after oil fractionation into saturates, aromatics, resins, and asphaltenes. Talanta 2008;74:1385–91. https://doi.org/10.1016/j.talanta.2007.09.009.

[21] Speight JG. Petroleum asphaltenes—Part 1: asphaltenes, resins and the structure of petroleum. Oil Gas Sci Technol Rev IFP 2004;59:467–77. https://doi.org/10.2516/ogst:2004032.

[22] Silva HS, Sodero AC, Bouyssiere B, et al. Molecular dynamics study of nanoaggregation in asphaltene mixtures: effects of the N, O, and S heteroatoms. Energy Fuels 2016;30:5656–64. https://doi.org/10.1021/acs.energyfuels.6b01170.

[23] Mullins OC. The Modified Yen Model. Energy Fuels 2010;24:2179–207. https://doi.org/10.1021/ef900975e.

[24] Groenzin H, Mullins OC. Molecular size and structure of asphaltenes from various sources. Energy Fuels 2000;14:677–84. https://doi.org/10.1021/ef990225z.

[25] Schuler B, Meyer G, Peña D, Mullins OC, Gross L. Unraveling the molecular structures of asphaltenes by atomic force microscopy. J Am Chem Soc 2015;137: 9870–6. https://doi.org/10.1021/jacs.5b04056.

[26] Zendehboudi S. Asphaltenes review: Characterization and modeling. In: Totten G, Shah R, Forester D, editors. Fuels and Lubricants Handbook: Technology, Properties, Performance, and Testing. 2nd ed. West Conshohocken, PA: ASTM International; 2019. p. 39–77. https://doi.org/10.1520/MNL3720160027.

[27] Mullins OC, Sabbah H, Eyssautier J, et al. Advances in asphaltene science and the Yen–Mullins model. Energy Fuels 2012;26:3986–4003. https://doi.org/10.1021/ef300185p.

[28] Lin Y, Cao T, Chacón-Patiño ML, Rowland SM, Rodgers RP, Yen A, et al. Microfluidic study of the deposition dynamics of asphaltene subfractions enriched with island and archipelago motifs. Energy Fuels 2019;33:1882–91. https://doi.org/10.1021/acs.energyfuels.8b03835.

[29] Hemmati-Sarapardeh A, Ameli F, Ahmadi M, Dabir B, Mohammadi A, Esfahanizadeh L. Effect of asphaltene structure on its aggregation behavior in toluene-normal alkane mixtures. J Mol Struct 2020;1220:128605. https://doi.org/10.1016/j.molstruc.2020.128605.

[30] Ghosh AK, Chaudhuri P, Kumar B, Panja SS. Review on aggregation of asphaltene vis-à-vis spectroscopic studies. Fuel 2016;185:541–54. https://doi.org/10.1016/j.fuel.2016.08.031.

[31] Evdokimov IN, Fesan AA, Losev AP. New answers to the optical interrogation of asphaltenes: monomers and primary aggregates from steady state fluorescence studies. Energy Fuels 2016;30:4494–503. https://doi.org/10.1021/acs.energyfuels.6b00027.

[32] Elkhatib O, Zhang B, Goual L. New insights into asphaltene structure and aggregation by high-resolution microscopy. Energy Fuels 2022;36:8692–700. https://doi.org/10.1021/acs.energyfuels.2c00925.

[33] Mahmoudvand S, Shahsavani B, Parsaei R, Malayeri MR. Prediction of asphaltene precipitation upon injection of various gases at near-wellbore conditions: a simulation study using PC-SAFT EoS. Oil Gas Sci Technol – Rev IFP Energ Nouv 2019;74:63. https://doi.org/10.2516/ogst/2019037.

[34] Hassanzadeh M, Abdouss M. Essential role of structure, architecture, and intermolecular interactions of asphaltene molecules on properties (self-association and surface activity). Heliyon 2022;8:e12170. https://doi.org/10.1016/j.heliyon.2022.e12170.

[35] Zekri Y, El-Mehaideb R. Steam/bacteria treatment of asphaltene deposition in carbonate rocks. J Petrol Sci Eng 2003;37:123–33. https://doi.org/10.1016/S0920-4105(02)00315-7.

[36] Hasanvand MZ, Ahmadi MA, Behbahani RM. Solving asphaltene precipitation issue in vertical wells via redesigning of production facilities. Petroleum 2015;1: 139–45. https://doi.org/10.1016/j.petlm.2015.07.002.

[37] Rogel E. Effect of inhibitors on asphaltene aggregation: a theoretical framework. Energy Fuels 2011;25:472–81. https://doi.org/10.1021/ef100912b.

[38] Ahmadi M, Chen Z. Molecular interactions between asphaltene and surfactants in a hydrocarbon solvent: Application to asphaltene dispersion. Symmetry 2020;12: 1767. https://doi.org/10.3390/sym12111767.

[39] Hashmi SM, Firoozabadi A. Effect of dispersant on asphaltene suspension dynamics: Aggregation and sedimentation. J Phys Chem B 2010;114:15780–8. https://doi.org/10.2118/135599-MS.

[40] Ahmadi MA, Chen Z. Challenges and future of chemical-assisted heavy oil recovery processes. Adv Colloid Interface Sci 2020;275:102081. https://doi.org/10.1016/j.cis.2019.102081.

[41] Kwon H, Go KS, Nho N-S, Kim KH. Effect of alkyl chain length of ionic surfactants on selective removal of asphaltene from oil sand bitumen. Energy Fuels 2018;32: 9304–13. https://doi.org/10.1021/acs.energyfuels.8b01933.

[42] Atta M, Abdullah MM, Al-Lohedan HA, Ezzat AO. Demulsification of heavy crude oil using new nonionic cardanol surfactants. J Mol Liq 2018;252:311–20. https://doi.org/10.1016/j.molliq.2017.12.154.

[43] Alhreez M, Wen D. Molecular structure characterization of asphaltene in the presence of inhibitors with nanoemulsions. RSC Adv 2019;9:19560–70. https://doi.org/10.1039/C9RA02664A.

[44] Ahmadi MA, Arabsahebi Y, Shadizadeh SR, Behbahani SS. Preliminary evaluation of mulberry leaf-derived surfactant on interfacial tension in an oil-aqueous system: EOR application. Fuel 2014;117:749–55. https://doi.org/10.1016/j.fuel.2013.08.081.

[45] Ahmadi MA, Shadizadeh SR. Spotlight on the new natural surfactant flooding in carbonate rock samples in low salinity condition. Sci Rep 2018;8:1–15. https://doi.org/10.1038/s41598-018-29321-w.

[46] Ahmadi MA, Shadizadeh SR. Nano-surfactant flooding in carbonate reservoirs: a mechanistic study. Eur Phys J Plus 2017;132:246. https://doi.org/10.1140/epjp/i2017-11488-6.

[47] Hu YF, Guo TM. Effect of the structures of ionic liquids and alkylbenzene-derived amphiphiles on the inhibition of asphaltene precipitation from CO_2-injected reservoir oils. Langmuir 2005;21:8168. https://doi.org/10.1021/la050212f.

[48] Ruiz-Morales YJ. HOMO−LUMO gap as an index of molecular size and structure for polycyclic aromatic hydrocarbons (PAHs) and asphaltenes: a theoretical study. Phys Chem A 2002;106:11283–308. https://doi.org/10.1021/jp021152e.

[49] Sirota EB. Physical structure of asphaltenes. Energy Fuels 2005;19:1290–6. https://doi.org/10.1021/ef049795b.

[50] Mirvakili A, Rahimpour MR, Jahanmiri A. Effect of a cationic surfactant as a chemical destabilization of crude oil based emulsions and asphaltene stabilized. J Chem Eng Data 2012;57:1689–99. https://doi.org/10.1021/je2013268.

[51] Goual L, Firoozabadi A. Effect of resins and DBSA on asphaltene precipitation from petroleum fluids. AIChE J 2004;50:470–9. https://doi.org/10.1002/aic.10041.

[52] Salmón-Vega S, Herrera-Urbina R, Lira-Galeana C, Valdez MA. The effect of ionic surfactants on the electrokinetic behavior of asphaltene from a Maya Mexican oil.

Pet Sci Technol 2012;30:986–92. https://doi.org/10.1080/10916466.2010.495966.
[53] Razipour M, Giri MS, Majidian N. Application of surfactants on asphaltene stability in heavy oil by interfacial tension approach. Energy Sources A: Recovery Util Environ Eff 2024;46:7201–13. https://doi.org/10.1080/15567036.2020.1752332.
[54] Wang M, Kaufman J, Chen X, Sungail C. Development and evaluation of non-ionic polymeric surfactants as asphaltene inhibitors. SPE Int Symp Oilfield Chem 2015; The Woodlands, TX, USA. DOI: 10.2118/173720-MS.
[55] Zhang H, Liu S, Wang X, Yuan S. Molecular dynamics study on emulsified oil droplets with nonionic surfactants. J Mol Liq 2022;346:117102. https://doi.org/10.1016/j.molliq.2021.117102.
[56] Ahmadi S, Khormali A, Kazemzadeh Y. A critical review of the phenomenon of inhibiting asphaltene precipitation in the petroleum industry. Processes 2025;13:212. https://doi.org/10.3390/pr13010212.
[57] Omari A, Cao R, Zhu Z, Xu X. A comprehensive review of recent advances on surfactant architectures and their applications for unconventional reservoirs. J Pet Sci Eng 2021;206:109025. https://doi.org/10.1016/j.petrol.2021.109025.
[58] Liang C, Liu X, Jia Y, Jiang H, Xu Y. Mechanistic study of the effects of surfactants and asphaltenes on the action of emulsions with different water contents: based on dissipative particle dynamics. Energy Fuels 2024;38:7758–72. https://doi.org/10.1021/acs.energyfuels.4c00363.
[59] Koczó K, Rácz G. Foaming properties of surfactant solutions. Colloids Surf 1991;56:59–82. https://doi.org/10.1016/0166-6622(91)80114-4.
[60] Krzan M, Kudłacik-Kramarczyk S, Drabczyk A, Kieres W. Foams based on biosurfactant mixtures. Part II. Influence of mixture composition on foam stability. Curr Opin Colloid. Interface Sci 2024;73:101825. https://doi.org/10.1016/j.cocis.2024.101825.
[61] Jiang J, Wang Z, Wang C, Shi L, Hou J, Zhang L. Effect of nonionic surfactants on the synergistic interaction between asphaltene and resin: Emulsion phase inversion and stability. Colloids Surf A Physicochem Eng Asp 2023;675:132056. https://doi.org/10.1016/j.colsurfa.2023.132056.
[62] Yang S, Wang H, Lou X, Pan Y, Hu Z, Yan Y. Asphaltene deposition inhibitors in CO2 flooding: a review and future application prospects. Energy Fuels 2024;38:22616–36. https://doi.org/10.1021/acs.energyfuels.4c03259.
[63] Mohammadi S, Rashidi F, Mousavi-Dehghani SA, Ghazanfari M-H. On the effect of temperature on precipitation and aggregation of asphaltenes in light live oils. Can J Chem Eng 2016;94(9):1820–9. https://doi.org/10.1002/cjce.22555.
[64] Forte E, Taylor SE. Thermodynamic modelling of asphaltene precipitation and related phenomena. Adv Colloid Interface Sci 2015;217:1–12. https://doi.org/10.1016/j.cis.2014.12.002.
[65] Al-Moubaraki AH, Obot IB. Corrosion challenges in petroleum refinery operations: sources, mechanisms, mitigation, and future outlook. J Saudi Chem Soc 2021;25(12):101370. https://doi.org/10.1016/j.jscs.2021.101370.
[66] Gawrys KL, Spiecker PM, Kilpatrick PK. The role of asphaltene solubility and chemical composition on asphaltene aggregation. Pet Sci Technol 2003;21(3):461–89. https://doi.org/10.1081/LFT-120018533.
[67] Ortiz RWP, Maravilha TSL, Belati A, Bispo FJS, Manoel EA, Oliveira Gonçalves VO, et al. Carboxylic acids in the synthesis of chemicals for addressing flow assurance challenges in offshore petroleum production. Curr Org Chem 2024;28(14):1102–17. https://doi.org/10.2174/0113852728305998240517074146.
[68] Ghlouma EF, Rasheda AM, Safaa MA, Sablitb RC, Al-Jouhara SM. Mitigation of asphaltenes precipitation phenomenon via chemical inhibitors. J Pet Sci Eng 2019;175:495–507. https://doi.org/10.1016/j.petrol.2018.12.071.
[69] Leon O, Contreras E, Rogel E, Dambakli G, Espidel J, Acevedo S. The influence of the adsorption of amphiphiles and resins in controlling asphaltene flocculation. Energy Fuels 2001;15(5):1028–32. https://doi.org/10.1021/ef010032n.
[70] Hashmi SM, Zhong KX, Firoozabadi A. Acid–base chemistry enables reversible colloid-to-solution transition of asphaltenes in non-polar systems. Soft Matter 2012;8:8778–85. https://doi.org/10.1039/C2SM26003D.
[71] Kashefi S, Shahrabadi A, Jahangiri S, Lotfollahi MN, Bagherzadeh H. Investigation of the performance of several chemical additives on inhibition of asphaltene precipitation. Energy Sources Part A 2016;38(24):3647–52. https://doi.org/10.1080/15567036.2016.1198847.
[72] Junior LCR, Ferreira MS, da Silva Ramos AC. Inhibition of asphaltene precipitation in Brazilian crude oils using new oil soluble amphiphiles. J Pet Sci Eng 2006;51(1–2):26–36. https://doi.org/10.1016/j.petrol.2005.11.006.
[73] Alhreez M, Wen D. Controlled releases of asphaltene inhibitors by nanoemulsions. Fuel 2018;234:538–48. https://doi.org/10.1016/j.fuel.2018.06.079.
[74] Lun Z, Liu Y, Zhang Q, Liu M, Liu J, Yang P. Study on inhibition behaviors of asphaltene inhibitor to asphaltene aggregations. J Dispers Sci Technol 2021;44(6):933–41. https://doi.org/10.1080/01932691.2021.1980001.
[75] Subramanian S, Simon S, Sjöblom J. Interaction between asphaltenes and fatty-alkylamine inhibitor in bulk solution. J Dispers Sci Technol 2017;39(2):163–73. https://doi.org/10.1080/01932691.2017.1304221.
[76] Zhang Q, Liu Y, Lun Z, Liu J, Zhang Y, Yang P. The study on interactions between stabilizers and asphaltenes. J Dispers Sci Technol 2022;45(3):461–74. https://doi.org/10.1080/01932691.2022.2158850.
[77] Kashefi S, Shahrabadi A, Jahangiri S, Lotfollahi MN, Bagherzadeh H. Investigation of the performance of several chemical additives on inhibition of asphaltene precipitation. Energy Sources Part A 2016;38(24):3647–52. https://doi.org/10.1080/15567036.2016.1198847.
[78] Wang J, Li C, Zhang L, Que G, Li Z. The properties of asphaltenes and their interaction with amphiphiles. Energy Fuels 2009;23(7):3625–31. https://doi.org/10.1021/ef801148y.
[79] Parra-Barraza H, Hernández-Montiel D, Lizardi J, Hernández J, Urbina RH, Valdez MA. The zeta potential and surface properties of asphaltenes obtained with different crude oil/n-heptane proportions. Fuel 2003;82(8):869–74. https://doi.org/10.1016/S0016-2361(03)00002-4.
[80] Kelland MA. Production chemicals for the oil and gas industry. CRC Press; 2016.
[81] Al-Taq AA, Alfakher BM, Al-Muhaish SA, Alrustum AA. From lab to field: an integrated approach to successfully restore the productivity of damaged wells with organic deposition. Abu Dhabi Int Petrol Exhib Conf Society of Petroleum Engineers 2016:D021S048R003. https://doi.org/10.2118/183539-MS.
[82] Al-Sahhaf TA, Fahim MA, Elkilani AS. Retardation of asphaltene precipitation by addition of toluene, resins, deasphalted oil and surfactants. Fluid Phase Equilib 2002;194:1045–57. https://doi.org/10.1016/S0378-3812(01)00702-6.
[83] Barcenas M, Orea P, Buenrostro-Gonzalez E, Zamudio-Rivera LS, Duda Y. Study of medium effect on asphaltene agglomeration inhibitor efficiency. Energy Fuels 2008;22(3):1917–22. https://doi.org/10.1021/ef700773m.
[84] Sedghi M, Goual L. Role of resins on asphaltene stability. Energy Fuels 2010;24(4):2275–80. https://doi.org/10.1021/ef9009235.
[85] Mullins OC, Sheu EY, Hammami A, Marshall AG. Asphaltenes, heavy oils, and petroleomics. New York: Springer; 2007.
[86] Rogel E, Leon O, Espidel Y, Gonzalez Y. Asphaltene stability in crude oils. SPE Prod Facil 2001;16(2):84–8. https://doi.org/10.2118/72050-PA.
[87] Schorling PC, Kessel DG, Rahimian I. Influence of the crude oil resin/asphaltene ratio on the stability of oil/water emulsions. Colloids Surf A 1999;152(1–2):95–102. https://doi.org/10.1016/S0927-7757(98)00686-4.
[88] Sjöblom J, Hemmingsen PV, Kallevik H. The role of asphaltenes in stabilizing water-in-crude oil emulsions. In: Mullins OC, Sheu EY, Hammami A, Marshall AG, editors. Asphaltenes, heavy oils, and petroleomics. Springer; 2007. DOI: 10.1007/0-387-68903-6_21.
[89] Moncayo-Riascos I, Taborda E, Hoyos BA, Franco CA, Cortés FB. Effect of resin/asphaltene ratio on the rheological behavior of asphaltene solutions in a de-asphalted oil and p-xylene: a theoretical–experimental approach. J Mol Liq 2020;315:113754. https://doi.org/10.1016/j.molliq.2020.113754.
[90] León O, Contreras E, Rogel E, Dambakli G, Acevedo S, Carbognani L, et al. Adsorption of native resins on asphaltene particles: a correlation between adsorption and activity. Langmuir 2002;18(13):5106–12. https://doi.org/10.1021/la011394q.
[91] Durand E, Clemancey M, Lancelin J-M, Verstraete J, Espinat D, Quoineaud A-A. Effect of chemical composition on asphaltenes aggregation. Energy Fuels 2010;24:1051–62. https://doi.org/10.1021/ef900599v.
[92] Hoepfner MP, Limsakoune V, Chuenmeechao V, Maqbool T, Fogler HS. A fundamental study of asphaltene deposition. Energy Fuels 2013;27:725–35. https://doi.org/10.1021/ef3017392.
[93] Yaseen S, Mansoori GA. Molecular dynamics studies of interaction between asphaltenes and solvents. J Pet Sci Eng 2017;156:118–24. https://doi.org/10.1016/j.petrol.2017.05.018.
[94] Chamkalani A, Zendehboudi S, Bahadori A, Kharrat R, Chamkalani R, James L, et al. Integration of LSSVM technique with PSO to determine asphaltene deposition. J Pet Sci Eng 2014;124:243–53. https://doi.org/10.1016/j.petrol.2014.10.001.
[95] Lyulin SV, Glova AD, Falkovich SG, et al. Computer simulation of asphaltenes Pet Chem 2018;58:983–1004. https://doi.org/10.1134/S0965544118120149.
[96] Tirjoo A, Bayati B, Rezaei H, Rahmati M. Molecular dynamics simulations of asphaltene aggregation under different conditions. J Pet Sci Eng 2019;177:392–402. https://doi.org/10.1016/j.petrol.2019.02.041.
[97] Hebbar A, Debraj D, Acharya S, Puttapati SK, Vatti AK, Dey P. Deep eutectic solvents interaction with asphaltenes: a combined experimental and molecular dynamics study. J Mol Liq 2023;387:122627. https://doi.org/10.1016/j.molliq.2023.122627.
[98] Yang S, Yan C, Cai J, Pan Y, Han Q. Research progress in nanoparticle inhibitors for crude oil asphaltene deposition. Molecules 2024;29(5):1135. https://doi.org/10.3390/molecules29051135.
[99] Vatti AK, Divi S, Dey P. Effectiveness of inhibitors to prevent asphaltene aggregation: Insights from atomistic and molecular simulations. J Chem Phys 2024;160(9):090901. https://doi.org/10.1063/5.0190779.
[100] Alemi FM, Mohammadi S, Mousavi Dehghani SA, Rashidi A, Hosseinpour N, Seif A. Experimental and DFT studies on the effect of carbon nanoparticles on asphaltene precipitation and aggregation phenomena. Chem Eng J 2021;422:130030. https://doi.org/10.1016/j.cej.2021.130030.
[101] Kumar N, Mohan M, Smith JC, Simmons BA, Singh S, Banerjee T. Inhibition of asphaltene aggregation using deep eutectic solvents: COSMO-RS calculations and experimental validation. J Mol Liq 2024;400:124471. https://doi.org/10.1016/j.molliq.2024.124471.
[102] Chávez-Miyauchi TE, Zamudio-Rivera LS, Barba-López V, Buenrostro-Gonzalez E, Martínez-Magadán JM. N-aryl amino-alcohols as stabilizers of asphaltenes. Fuel 2013;110:302–9. https://doi.org/10.1016/j.fuel.2012.10.044.
[103] ASTM International. Standard Test Method for Determination of Asphaltenes (Heptane Insolubles) in Crude Petroleum and Petroleum Products, ASTM D6560-12. 2018.
[104] Yolchuyeva UJ, Abbasov VM, Jafarova R, Mammadov AM, Ahmadbayova S, Rahimov RA, et al. Chemical composition and molecular structure of asphaltene in Azerbaijani crude oil: a case study of the Zagli field. Fuel 2024;373:132084. https://doi.org/10.1016/j.fuel.2024.132084.
[105] Asadov ZH, Rahimov RA, Mammadova KA, Ahmadova GA, Ahmadbayova SF. Synthesis and Colloidal-Chemical Properties of Surfactants based on Alkyl Amines and propylene Oxide. Tenside Surf Det 2015;52(4). https://doi.org/10.3139/113.110377.

[106] Frisch MJ, Trucks GW, Schlegel HB, Scuseria GE, Robb MA, Cheeseman JR, et al. Gaussian 16, Revision C.01. Gaussian Inc., Wallingford CT; 2016.
[107] Hehre WJ, Ditchfield R, Pople JA. Self–consistent molecular orbital methods. XII. further extensions of Gaussian–type basis sets for use in molecular orbital studies of organic molecules. Chem Phys 1972;56:2257–61. https://doi.org/10.1063/1.1677527.
[108] Grimme S, Antony J, Ehrlich S, Krieg H. A consistent and accurate ab initio parametrization of density functional dispersion correction (DFT-D) for the 94 elements H-Pu. J Chem Phys 2010;132:154104. https://doi.org/10.1063/1.3382344.
[109] Boys SF, Bernardi F. The calculation of small molecular interactions by the differences of separate total energies. some procedures with reduced errors. Mol Phys 1970;19:553–66. https://doi.org/10.1080/00268977000101561.
[110] Lu T, Chen F. Multiwfn: a multifunctional wavefunction analyzer. J Comput Chem 2012;33:580–92. https://doi.org/10.1002/jcc.22885.
[111] Williams CK Thomas. http://www.gnuplot.info/ (2004).
[112] Humphrey W, Dalke A, Schulten KVMD. Visual molecular dynamics. J Mol Graph 1996;14:33–8. https://doi.org/10.1016/0263-7855(96)00018-5.
[113] Asemani M, Rabbani AR. Detailed FTIR spectroscopy characterization of crude oil extracted asphaltenes: Curve resolve of overlapping bands. J Pet Sci Eng 2019;106618. https://doi.org/10.1016/j.petrol.2019.106618.
[114] Parra-Barraza H, Hernández-Montiel D, Lizardi J, Hernández J, Urbina RH, Valdez MA. The zeta potential and surface properties of asphaltenes obtained with different crude oil/n-heptane proportions. Fuel 2003;82:869–74.
[115] Wang Y, Xia TD, Zheng H, Feng HX. Stearic acid/silica fume composite as form-stable phase change material for thermal energy storage. Energ Buildings 2011;43:2365–70.
[116] Ok S, Rajasekaran N, Sabti MA, Joseph GA. Spectroscopic analysis of crude oil asphaltenes at molecular level. Pet Chem 2020;60(7):802–9. https://doi.org/10.1134/S0965544120070117.
[117] Zojajia I, Esfandiarian A, Taheri-Shakib J. Toward molecular characterization of asphaltene from different origins under different conditions by means of FT-IR spectroscopy. Adv Colloid Interface Sci 2021;289:102314. https://doi.org/10.1016/j.cis.2020.102314.
[118] Buenrostro-Gonzalez E, Andersen SI, Garcia-Martinez JA, Lira-Galeana C. Solubility/molecular structure relationships of asphaltenes in polar and nonpolar media. Energy Fuels 2002;16(3):732–41. https://doi.org/10.1021/ef0102317.
[119] da Silva Oliveira EC, Cunha Neto Á, Lacerda Júnior V, Ribeiro de Castro EV, Cabral de Menezes SM. Study of Brazilian asphaltene aggregation by Nuclear magnetic Resonance spectroscopy. Fuel 2014;117:146–51. https://doi.org/10.1016/j.fuel.2013.09.022.
[120] Behnous D, Bouhadda Y, Moffatt B, Zeraibi N, Coutinho JAP. Chemical characterization of asphaltenes deposits from Hassi Messaoud field. Fuel 2022;328:125305. https://doi.org/10.1016/j.fuel.2022.125305.
[121] Yolchuyeva U, Japharova R, Khamiyev M, Alimardanova F. Investigation of Surakhani light crude oil compounds as a case study using modern spectroscopic techniques. J Pet Explor Prod Technol 2024;14(1):289–302. https://doi.org/10.1007/s13202-023-01702-6.
[122] Yolchuyeva U, Jafarova R, Khamiyev M, Vakhshouri AR, Khamiyev G. Investigation of photochemical conversion processes in aromatic hydrocarbons of Balakhani oil. J Pet Sci Eng 2021;196:108089. https://doi.org/10.1016/j.petrol.2020.108089.
[123] Esmaeilian N, Rabiei N, Mahmoudi M, Dabir B. Asphaltene structure determination: FTIR, NMR, EA, ICP-OES, MS, XRD and computational chemistry considerations. J Mol Liq 2023;385:122279. https://doi.org/10.1016/j.molliq.2023.122279.
[124] Ok S, Mal T. NMR Spectroscopy Analysis of Asphaltenes. Energy Fuels 2019;33(11):10391–414. https://doi.org/10.1021/acs.energyfuels.9b02240.
[125] Davarpanah L, Vahabzadeh F, Dermanaki A. Structural Study of Asphaltenes from Iranian Heavy Crude Oil. Oil Gas Sci Technol –. Rev IFP Energies nouvelles 2015;70:1035–49. https://doi.org/10.2516/ogst/2012066.
[126] Vuković JP, Novak P, Jednačak T. NMR Spectroscopy as a Tool for Studying Asphaltene Composition. Croat Chem Acta 2019;92(3):323–9. https://doi.org/10.5562/cca3543.
[127] Ok S, Mahmoodinia M, Rajasekaran N, Sabti MA, Lervik A, van Erp TS, et al. Molecular Structure and Solubility Determination of Asphaltenes. Energy Fuels 2019;33(9). https://doi.org/10.1021/acs.energyfuels.9b01737.
[128] Simon S, Wei D, Barriet M, Sjöblom J. An ITC and NMR study of interaction and complexation of asphaltene model compounds in apolar solvent I: Self-association pattern. Colloids Surf A Physicochem Eng Asp 2016;494:108–15. https://doi.org/10.1016/j.colsurfa.2016.01.018.
[129] Baudot A, Cacela C, Duarte ML, Fausto R. Thermal study of simple amino-alcohol solutions. Cryobiology 2002;44(2):150–60. https://doi.org/10.1016/S0011-2240(02)00017-2.
[130] Lababidi HMS, Sabti HM, AlHumaidan FS. Changes in asphaltenes during thermal cracking of residual oils. Fuel 2014;117:59–67. https://doi.org/10.1016/j.fuel.2013.09.048.
[131] AlHumaidan FS, Hauser A, Rana MS, Lababidi HMS. Impact of thermal treatment on Asphaltene functional groups. Energy Fuels 2016;30:2892–903. https://doi.org/10.1021/acs.energyfuels.6b00261.
[132] Banda EE, Rivas NV, Páramo U, Estrada IA, Pozas D, Reyes J. Crude oil aggregation by microscopy and dynamic light scattering. Pet Sci Technol 2016;34(22):1812–917. https://doi.org/10.1080/10916466.2016.1230754.
[133] Paridar S, Solaimany Nazar AR, Karimi Y. Experimental evaluation of asphaltene dispersants performance using dynamic light scattering. J Pet Sci Eng 2018;163:570–5. https://doi.org/10.1016/j.petrol.2018.01.013.
[134] AlHumaidan FS, Rana MS, Tanoli NJ, Lababidi HMS, Al-Najdi NA. Changes in Asphaltene Surface Topography with thermal Treatment. Arab J Chem 2020;13(5):5377–89. https://doi.org/10.1016/j.arabjc.2020.03.016.
[135] Davarpanah L, Vahabzadeh F, Dermanaki A. Structural study of asphaltenes from iranian heavy crude oil. Oil Gas Sci Technol – Rev IFP Energies nouvelles 2015;70(6):1035–49. https://doi.org/10.2516/ogst/2012066.
[136] Nagy PI, Erhardt PW. On the Interaction of Aliphatic Amines and ammonium Ions with Carboxylic Acids in solution and in Receptor pockets. J Phys Chem B 2012;116:5425–36. https://doi.org/10.1021/jp300588q.